Journal of Molecular Graphics and Modelling 38 (2012) 155–164

Contents lists available at SciVerse ScienceDirect

Journal of Molecular Graphics and Modelling

journal homepage: www.elsevier.com/locate/JMGM

Ligand-specific homology modeling of human cannabinoid (CB1) receptor

Rizi Ai, Chia-en A. Chang*

Department of Chemistry, University of California Riverside, Riverside, CA 92521, USA

ARTICLE INFO

Article history:
Accepted 15 May 2012
Available online 31 May 2012

Keywords:
G-protein coupled receptors (GPCRs)
Protein–drug interactions
Membrane proteins
Computer-aided drug design
Binding

ABSTRACT

Cannabinoid (CB1) receptor is a therapeutic drug target, and its structure and conformational changes after ligand binding are of great interest. To study the protein conformations in ligand bound state and assist in drug discovery, CB1 receptor homology models are needed for computer-based ligand screening. The known CB1 ligands are highly diverse structurally, so CB1 receptor may undergo considerable conformational changes to accept different ligands, which is challenging for molecular docking methods. To account for the flexibility of CB1 receptor, we constructed four CB1 receptor models based on four structurally distinct ligands, HU-210, ACEA, WIN55212-2 and SR141716A, using the newest X-ray crystal structures of human β_2 adrenergic receptor and adenosine A_{2A} receptor as templates. The conformations of these four CB1–ligand complexes were optimized by molecular dynamics (MD) simulations. The models revealed interactions between CB1 receptor and known binders suggested by experiments and could successfully discriminate known ligands and non-binders in our docking assays. MD simulations were used to study the most flexible ligand, ACEA, in its free and bound states to investigate structural mobility achieved by the rearrangement of the fatty acid chain. Our models may capture important conformational changes of CB1 receptor to help improve accuracy in future CB1 drug screening.

1. Introduction

Cannabinoid (CB1) receptor belongs to class A G-protein coupled receptors (GPCRs) that represent the largest membrane protein family and are of great pharmacological importance. Currently, nearly one-third of marketed pharmaceuticals target GPCRs [1]. CB1 receptor is a therapeutically useful target involved in a wide variety of physiological processes, including metabolic regulation, craving, pain, and anxiety [2,3]. Licensed drugs target cannabinoid receptors for treating chemotherapy-induced nausea and vomiting, relieving neuropathic pain, and as an appetite stimulant for AIDS patients [4]. Drugs targeting CB1 receptor are continually being developed [5–8].

Because no crystal structure of CB1 receptor is available, computational methods have been used to model the receptor [9–12]. Up to late 2007, the CB1 receptor model was built based on bovine rhodopsin, a GPCR, because of its available high-resolution structure as a template for CB1 receptor modeling [10,11,13–16]. In recent years, with more GPCR structures being crystallized, new templates such as human adenosine A_{2A} receptor ($AA_{2A}R$) and β_2 adrenergic receptor (β_2AR) have become available [12,17,18]. The X-ray structures of different GPCRs share overall topology, but local structures can differ [19]. Molecular dynamics (MD) simulations and docking methods have been used to further study the conformational changes of CB1 receptor and the interactions between ligands and CB1 receptor. MD simulations of CB1 receptor embedded in a lipid bilayer have been used to gain insight into the interhelical and protein–ligand interactions [17,20,21]. Because we lack ligand–CB1 receptor experimental structures, mutation experiments are commonly used to help determine functional residues that affect ligand binding and can be guidelines to evaluate modeling results [9,22–25].

Cannabinoid ligands are highly diverse structurally. CB1 agonists can be classified into four groups: classical cannabinoids (1, 2, Fig. 1), non-classical cannabinoids (3, 4, Fig. 1), endogenous cannabinoids (5, Fig. 1) and aminoalkylindoles (7, 8, Fig. 1). CB1 antagonists/inverse agonists are diarylpyrazoles (9, 10, Fig. 1) or in other chemical series [26]. Representative ligands in each group are in Fig. 1. The groups differ greatly in constitution of rings and hydrocarbon chains. Although the endogenous cannabinoids do not have a ring conformation, the flexible long hydrocarbon chains can adopt conformations with high affinities.

In this study, in order to study protein conformational changes in the ligand bound states and consider the flexibility of CB1 receptor for drug screening, we constructed four CB1 receptor homology models based on four structurally different tight binders: (−)-11-hydroxydimethylheptyl-Δ^8-tetrahydrocannabinol (HU-210) (2, Fig. 1), arachidonyl-2-chloroethylamide (ACEA) (6, Fig. 1), (R)-(+)-[2,3-dihydro-5-methyl-3-[(4-morpholinyl)methyl]pyrrolo[1,2,3-de]-1,4-benzoxazin-6-yl](1-naphthalenyl)methanone (WIN55212-2) (7, Fig. 1) and

* Corresponding author. Tel.: +1 9518277263; fax: +1 9518272040.
E-mail address: chiaenc@ucr.edu (C.-e.A. Chang).

1093-3263/$ – see front matter © 2012 Elsevier Inc. All rights reserved.
http://dx.doi.org/10.1016/j.jmgm.2012.05.002

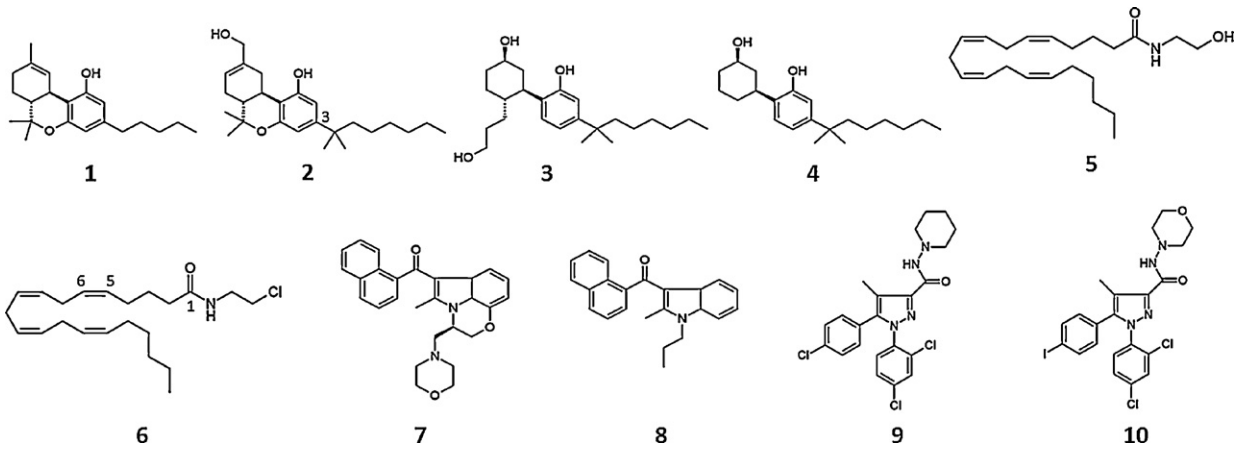

Fig. 1. Molecular structures of cannabinoid ligands in (1, 2) classical cannabinoids, (3, 4) non-classical cannabinoids, (5) endogenous cannabinoids, (7, 8) aminoalkylindoles and (9, 10) diarylpyrazoles. (1) (−)-Δ^9-THC, (2) HU-210, (3) CP55940, (4) CP47497, (5) anadamide, (6) ACEA, (7) WIN55212-2, (8) JWH-015, (9) SR141716A, (10) AM281.

N-(piperidin-1-yl)-5-(4-chlorophenyl)-1-(2,4-dichlorophenyl)-4-methyl-1H-pyrazole-3-carboxamide (SR141716A) (9, Fig. 1). The classical cannabinoid agonist HU-210 is a structural analog of (−)-Δ^9-tetrahydrocannabinol (THC) (1, Fig. 1) but with higher binding affinity. Because the classical and non-classical cannabinoids share overall structural features, HU-210 was selected to represent ligands in these two groups. ACEA is a selective CB1 agonist that is an endogenous cannabinoid analog but with higher binding affinity than a natural ligand anadamide (AEA) (5, Fig. 1). WIN55212-2 is a typical aminoalkylindole, and SR141716A is the first reported CB1 antagonist to display nanomolar CB1 receptor affinity [7]. We first constructed homology models using the newest GPCR crystal structures, β_2AR and AA_{2A}R, as templates and then used MD simulations and protein threading to train the models. To reveal changes in ligand flexibility in the free and bound states, motions of key ACEA dihedral angles were analyzed [27]. Since SR141716A is an antagonist to CB1 receptor, whole-protein MD simulations was used to adjust the model for antagonist/inverse agonist binding. The models can successfully discriminate known binders, compounds that are structurally similar to the binders and randomly chosen compounds by molecular docking and re-scoring.

2. Methods

2.1. Homology modeling

Construction of CB1 receptor homology models involved several essential steps. First, human brain CB1 protein sequence (GI: 237681175) was downloaded from the NCBI protein database (http://www.ncbi.nlm.nih.gov/protein). Two templates, β_2AR (PDB code: 3KJ6) and AA_{2A}R (PDB code: 3EML), were selected to construct CB1 model [28,29]. For multiple sequence alignment, GPCRs with similar protein sequences as CB1 receptor were identified by gapped BLAST search and HHSearch in template library of SWISS-MODEL [30,31]. Multiple sequence alignment was performed at T-Coffee (http://www.ebi.ac.uk/Tools/t-coffee/) using sequences of bovine rhodopsin (PDB code: 1F88 and 1U19), β_2AR (PDB code: 2R4R, 2RH1 and 3KJ6) and AA_{2A}R (PDB code: 3EML) (Table 1) [32–36]. To ensure that the alignment correctly placed the sequences of transmembrane helices (TMHs), PsiPred for secondary-structure prediction of CB1 receptor was used as guidelines to correct alignment [37]. Finally, with the two selected templates and the multiple sequence alignment, SWISS-MODEL (http://swissmodel.expasy.org/) *Alignment Mode* was used for CB1 receptor homology modeling [38]. Two models were built initially; one is based on template β_2AR and the other is based on template AA_{2A}R.

2.2. Model refinement

To further refine the transmembrane region of CB1 model, each helix and loop fragment was also constructed individually by SWISS-MODEL. The shape of each individually built helix in the transmembrane region was compared with models generated with the full-length CB1 protein sequence by two templates (AA_{2A}R and β_2AR). Based on the templates and PsiPred secondary-structure prediction, the best-shaped helix and loop pieces were isolated and assembled into a new hybrid model (Supplementary Material, Fig. S1) [37]. For example, helix 1 was built by template AA_{2A}R (Fig. S1, A1), template β_2AR (Fig. S1, A2) and individual helix 1 fragment (Fig. S1, A3). The beginning part of helix 1 built by template AA_{2A}R (Fig. S1, A1) did not show well-shaped helix compared to the other two structures which are both well-constructed. Therefore, helix 1 structure constructed by template β_2AR (Fig. S1, A2) was selected for CB1 model. In addition, helix 2 and 3 were further modified by MD simulations and protein threading. Finally, we adopted the conformation generated by protein threading at WURST (http://www.zbh.uni-hamburg.de/wurst/) (see Supplementary Material, Table S1) [39].

After generating the backbone, sidechains were added by use of SCWRL4 [40]. Quick conjugate gradients energy minimization and MD simulations were performed on CB1 hybrid model by NAMD/VMD in AMBER force field [41–43]. Because this study focuses on the ligand binding site, extensive loop conformational search was not performed [44,45].

2.3. Modeling the binding site by four types of ligands

To more accurately construct the binding site of CB1 receptor, CB1 models were further optimized by four tight binders of CB1 receptor, HU-210, ACEA, WIN55212-2 and SR141716A, using MD simulations. Before optimizing, the CB1 model underwent MD simulations, with explicit water molecules included only in the protein binding site. After that, HU-210 was docked to the binding site of CB1 model using Vdock to obtain the initial conformation for MD simulations [46]. Antechamber in AmberTools was used to assign parameters to the ligand–protein complex [47]. MD simulations were carried out using the NAMD package implemented in VMD, with Amber ff99SB and general Amber force field (GAFF) for CB1 receptor and ligands, respectively [41–43]. All MD simulations were performed under the NVT ensemble at 300 K with

Table 1
Sequence alignment of helix regions of multiple GPCR sequences.

Helix	Start residue		Sequence Alignment	End residue
1	35	1U19	PWQFSMLAAYMFLLIMLGFPINFLTLYVTVQ	65
	23	3EML	VY---ITVELAIAV-LA-ILGNVLVCWAVWL	48
	32	3KJ6	VWVVGMGIVMSLIV-LAIVFGNVLVITAIAK	61
	113	CB1	PSQQLAIAVLSLTLGTFTVLENLLVLCVILH	143
2	72	1U19	PLN-YILLNLAVADLFMVFG-GFTTTLYTSL	100
	55	3EML	VTN-YFVVSLAAADIAVGVL-AIPFA--ITI	81
	68	3KJ6	VTN-YFITSLACADLVMGLA-VVPFGAAHIL	96
	150	CB1	RPSYHFIGSLAVADLLGSVIFVYSFIDFHVF	180
3	106	1U19	FGPTGCNLEGFFATLGGEIALWSLVVLAIERYVVVC	141
	87	3EML	AACHGCLFIACFVLVLTQSSIFSLLAIAIDRYIAIR	122
	102	3KJ6	FGNFWCEFWTSIDVLCVTASIETLCVIAVDRYFAIT	137
	186	CB1	RNVFLFKLG--GVTASFTASVGSLFLTAIDRYISIH	219
4	151	1U19	ENHAIMGVAFTWVMALACAA-PPLVG	175
	133	3EML	GTRAKGIIAICWVLSFAIGL-TPMLG	157
	148	3KJ6	KNKARVIILMVWIVSGLTSFLPIQMH	173
	230	CB1	RPKAVVAFCLMWTIAIVIAVL-PLLG	254
5	201	1U19	NESFVIY-MFVVHFIIPLIVIFFCYGQLVFTVKEAAAQQ	238
	188	3EML	PMNYMVYFNFFACVLVPLLLMLGVYLRIFLAARRQ----	222
	197	3KJ6	NQAYAIA-SSIVSFYVPLVIMVFVYSRVFQEAKRQ----	230
	272	CB1	DETYLMFW-IGVT-SVLLLFIVYAYMYILWKAHSHAVRM	308
6	246	1U19	KAEKEVTRMVIIMVIAFLICWLPYAGVAFYIFT	278
	389	3EML	KEVHAA-KSLAIIVGLFALCWLPLHIINCFTFF	420
	268	3KJ6	KEHKAL-KTLGIIMGTFTLCWLPFFIVNIVHVI	299
	337	CB1	MDIRLA-KTLVLILVVLIICWGPLLAIMVYDVF	368
7	285	1U19	GPIFMTI-PAFFAKTSAVYNPVIYIM	309
	427	3EML	APLWLMYLAIVLSHTNSVVNPFIYAY	452
	306	3KJ6	KEVY-ILL-NWIGYVNSGFNPLIYC-	328
	376	CB1	KTVF-AFC-SMLCLLNSTVNPIIYAL	399
8	312	1U19	KQFRNCMVTTL	322
	455	3EML	REFRQTFRKII	465
	331	3KJ6	PDFRIAFQELL	341
	402	CB1	KDLRHAFRSMF	412

GPCR sequences included rhodopsin (PDB code: 1U19), β_2 adrenergic receptor (β_2AR; PDB code: 3KJ6), human adenosine A_{2A} receptor ($AA_{2A}R$; PDB code: 3EML) and CB1 receptor, shown in helix regions only. Conservancy of the aligned sequence is represented by consensus symbols: "*" for identical residues (red); "**:**" for conserved substitutions (cyan); and "**.**" for semi-conserved substitutions (yellow).

a time step of 1 fs. Residues within 12 Å of HU-210 were set as mobilized. When CB1 receptor was in the ligand free state, several polar residues, such as K3.28(192), formed hydrogen bonds with themselves and neighboring residues. To more efficiently relax the sidechain conformations, residues within 12 Å of HU-210 were heated to 500 K shortly (around 0.1 ns) each time to rearrange sidechain conformations and re-form proper ligand–CB1 receptor intermolecular interactions. The system was then followed by 1000 steps quick energy minimization and longer MD simulations in 300 K to prevent secondary structure changes. MD simulations were performed at 500 K and 300 K alternately and in total 1.2 ns at 500 K and 5.2 ns at 300 K. Afterwards, quick conjugate gradients energy minimization (1000–3000 steps) in AMBER force field was used to obtain a local energy minimum conformation of the CB1 receptor model for molecular docking studies [43].

We optimized the other three CB1 models using ACEA, WIN55212-2 and SR141716A with the same procedure described in Section 2.3. Root-mean-square deviation (RMSD) of residues that were within 12 Å of ACEA during MD simulations of ACEA–CB1 complex is shown in Supplementary Material, Fig. S2. Since SR141716A is an antagonist for CB1 receptor, training the CB1 model based on SR141716A toward inactive state was necessary. Since both WIN55212-2 and SR141716A share certain structural similarities and were identified to share the same microdomain in CB1 receptor [9], we constructed inactive CB1 receptor model using the initial model trained by WIN55212-2. Four ns whole-protein MD simulations were used to adjust the model for antagonist/inverse agonist binding.

2.4. Model verification

Four CB1 receptor models were then tested by docking known binders, compounds that are structurally similar to the known binders and random compounds with Vdock [46]. AutoDock 4 and AutoDock Vina were also used; however, both programs failed to dock ACEA ligand, so we reported only results from Vdock [48,49]. Structures of CB1 binders are listed in Supplementary Material, Fig. S3. Compounds with similar structures to each known binder were selected by substructure search and similarity search (similarity = 50%) from the ZINC database (Fig. 2) [50]. The resulting compounds were further screened to avoid highly similar structures. For example, compounds that are structurally similar to HU-210 were selected using substructure search (Fig. 2A1–4) and similarity search (similarity = 50%) from the ZINC database and 59 of them (Table 2) were picked to dock to the CB1 model trained by HU-210. In addition, 25 random compounds (Supplementary

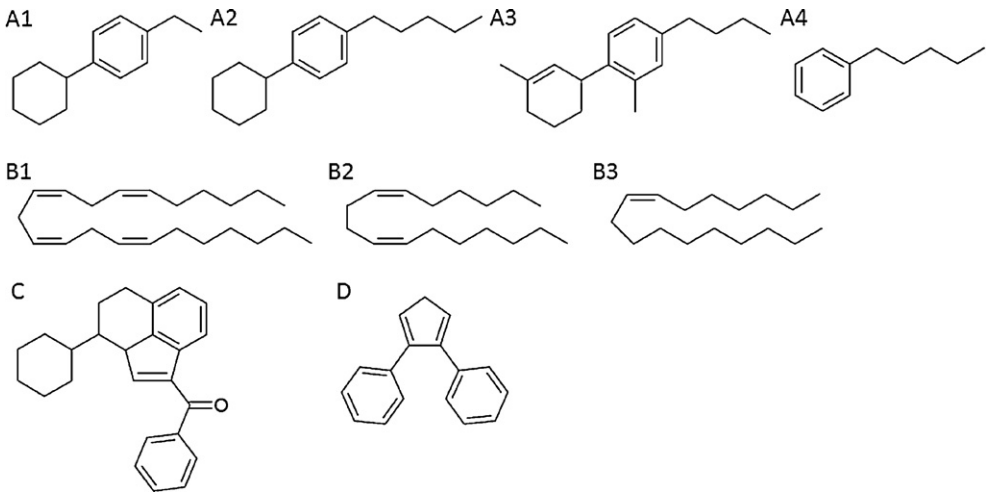

Fig. 2. Substructures of (A1–4) HU-210, (B1–3) ACEA, (C) WIN55212-2 and (D) SR141716A used for substructure search in the ZINC database.

Material, Fig. S4) were chosen from the NCI diversity set II (http://dtp.nci.nih.gov/branches/dscb/div2_explanation.html).

2.5. Energy calculation

In addition to docking, energy calculation was applied for re-scoring. In total, 3000 steps of energy minimization were used to relax the binding sites of the best-docked ligand–CB1 complexes. Total energy (E) was calculated by NAMDEnergy in VMD [42]. Binding energy between protein and ligand was calculated as follows:

$$\Delta E_{bind} = E_{complex} - (E_{protein} + E_{ligand})$$

Because ligands that are similar to HU-210 are smaller than other types of CB1 ligands, for the CB1 model optimized by HU-210, 500–1000 steps, instead of 3000 steps, of energy minimization were used before energy calculation. The minimization was terminated when the dihedral energy reached a plateau.

2.6. Flexibility analysis of ACEA

To study motions of the unsaturated acyl chain of ACEA, we used T-Analyst [27] to analyze the flexibility of each rotatable bond for trajectories from MD simulations. We performed three 3 ns MD simulations for ACEA in different environments: ACEA–CB1 bound state, free ACEA in a 10 Å × 10 Å × 10 Å cubic TIP3P water box, and free ACEA in vacuum. Frames were saved every 3 ps, for a total of 1000 frames. The MD simulations all started from the same initial ACEA conformation, with a folded structure from the ligand bound state. The configurational entropy of 17 dihedral angles of ACEA was computed using T-Analyst.

3. Results and discussion

3.1. CB1 receptor models

In considering ligand-induced conformational changes in the binding site of CB1 receptor and the highly diverse structures of CB1 ligands, we constructed four CB1 receptor models based on four types of ligands: HU-210, ACEA, WIN55212-2 and SR141716A. The four CB1 ligands are in similar positions in the binding sites (Fig. 3). However, because the compounds have various scaffolds, the backbones of the four CB1 receptor models are slightly different to accommodate the ligands.

3.1.1. CB1 model trained by HU-210

HU-210 is an analog to (−)-Δ^9-THC, with higher binding affinity than natural THC, so it was selected to represent structurally similar classical and non-classical cannabinoids. In this model, HU-210 binds to the TMH3-6-7 region of CB1 receptor. The alkyl chain of HU-210 points to the inside of the binding cavity and locates near I6.46(354), C6.47(355), W6.48(356), L6.51(359) and L6.52(360), and the tricyclic scaffold of HU-210 is toward F2.64(177), F3.25(189), K3.28(192), M6.55(363), F7.35(379) and

Table 2
Average interaction energy of known CB1 binders, compounds structurally similar to binders and random compounds in the four CB1 models (kcal/mol).

Model	Binders		Compounds with similar binder structures[a]		Random compounds[b]	
	No.	Binding energy	No.	Binding energy	No.	Binding energy
HU-210 model	3[d]	−50.43 ± 1.37	59	−36.73 ± 7.57	22	−31.58 ± 9.39
					3	Failed to dock[c]
ACEA model	5[d]	−62.42 ± 2.81	15	−48.94 ± 13.56	23	−44.43 ± 13.23
			5	Failed to dock[c]	2	Failed to dock[c]
WIN55212-2 model	2[e]	−62.12 ± 5.82	36	−45.12 ± 9.76	24	−44.63 ± 14.6
			3	Failed to dock[c]	1	Failed to dock[c]
SR141716A model	5[f]	−66.53 ± 6.10	38	−50.59 ± 11.98	20	−37.83 ± 11.83
			27	Failed to dock[c]	5	Failed to dock[c]

[a] Compounds structurally similar to binders were selected by substructure and similarity search (similarity = 50%) from ZINC database.
[b] Random compounds were chosen from the NCI diversity set II.
[c] Docking failed because the docking software failed to dock the ligand in the binding site of the protein or the ligand was docked in an inappropriate position.
[d] Ref. [21].
[e] Ref. [50].
[f] Ref. [51].

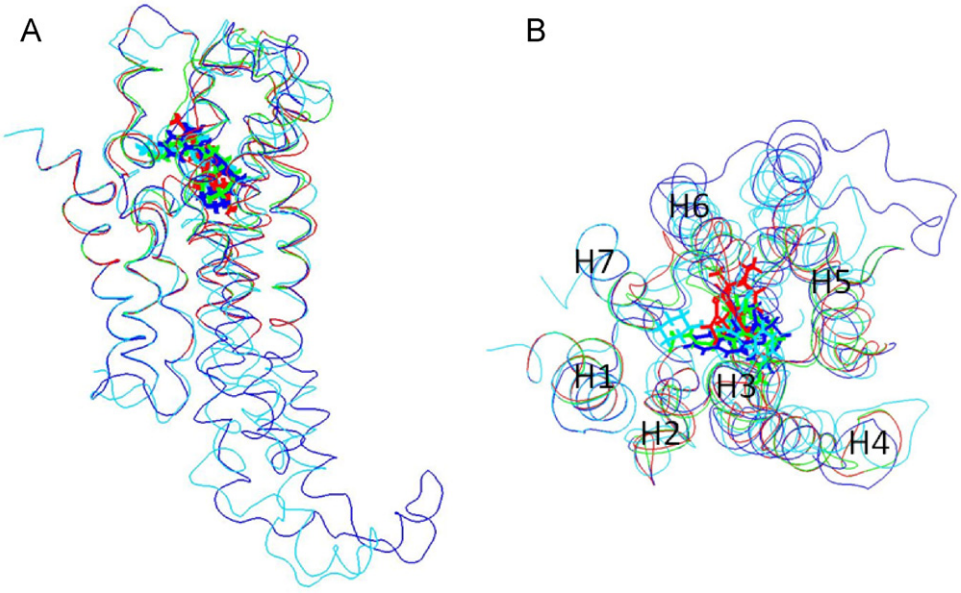

Fig. 3. Alignment of the four ligand–CB1 models. (A) Side view. (B) Top view. Seven transmembrane helices are indicated (H1–7). Colors represent models trained by HU-210 (red), ACEA (green), WIN55212-2 (blue) and SR141716A (cyan).

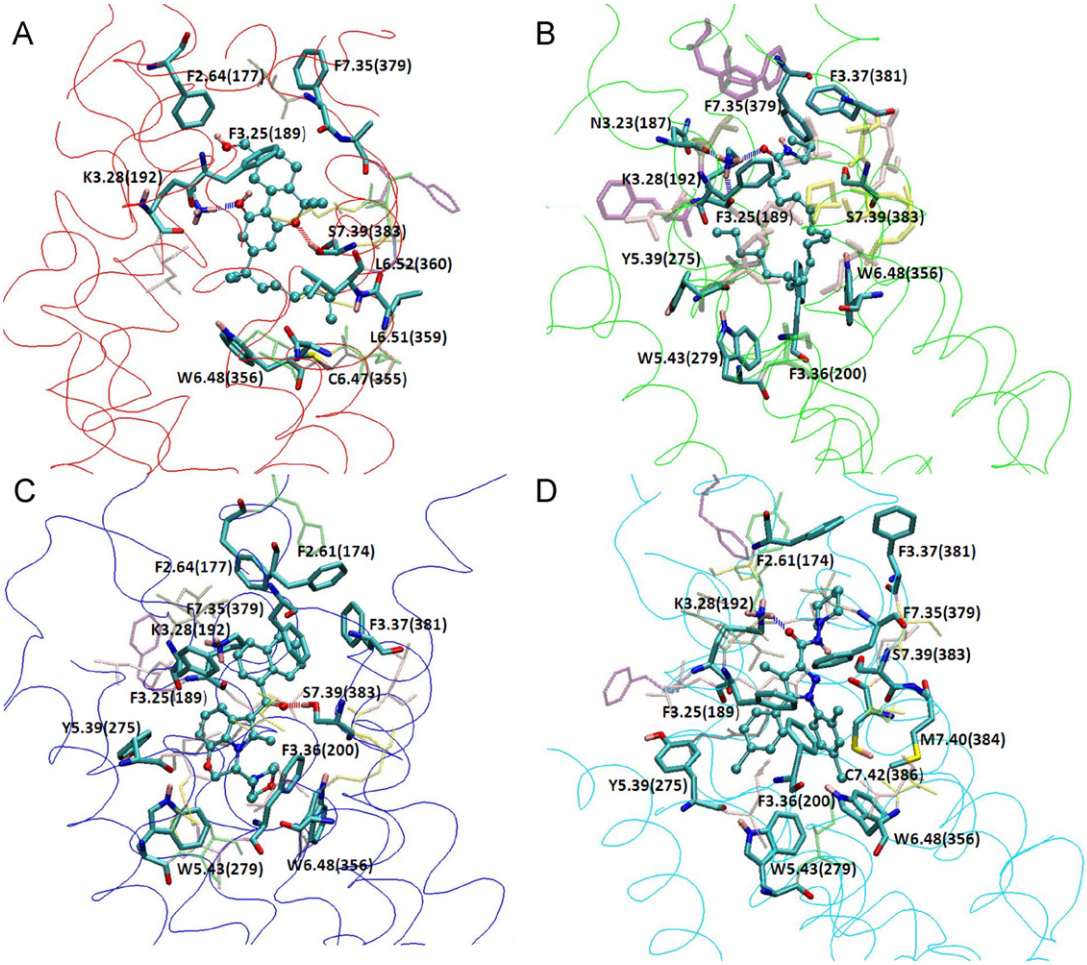

Fig. 4. Binding sites of CB1 receptor models trained by (A) HU-210, (B) ACEA, (C) WIN55212-2 and (D) SR141716A. Ligands are in ball-and-stick depiction. Residues that that are directly contact with ligands are in opaque stick depiction. Residues that are within 6 Å of the ligands are in transparent stick depiction (see Supplementary Material, Table S3 for details).

S7.39(383) (Fig. 4A). Mutation study [22] showed K3.28(192) is an important residue involved in HU-210 binding, and the phenolic oxygen of HU-210 formed a hydrogen bond with K3.28(192) in our complex conformation. In addition, the binding affinity of HU-210 was reduced 50- to 100-fold when mutating S7.39(383) to alanine [24]. In our model, K3.28(192) acts as a hydrogen bond donor to F3.25(189) which locates near the tricyclic scaffold of HU-210 and helps stabilize HU-210 binding. The pyranyl oxygen of HU-210 acts as a hydrogen bond acceptor to S7.39(383). Besides, C6.47(355) is in close contact with the end of the alkyl chain of HU-210, which is also consistent with previous docking and site-directed mutagenesis study [51].

3.1.2. CB1 model trained by ACEA

ACEA is a selective CB1 agonist that is structurally similar to endogenous cannabinoids such as AEA but with higher binding affinity. The long unsaturated acyl chain distinguishes itself from other groups of cannabinoid ligands. In our model, ACEA binds to TMH2-3-6-7 region and adopted a folded J-shape to form hydrophobic intermolecular contacts with CB1 receptor. U-shaped endocannabinoids conformations were also found in others studies [11,16]. ACEA is located at the lipophilic region of the binding site and in the vicinity of residues such as K3.28(192), S7.39(383), F3.25(189), F7.35(379), F7.37(381), Y5.39(275), F3.36(200) and W6.48(356). According to mutation study, K3.28(192) is a critical residue for AEA binding [22], and the carbonyl oxygen of ACEA formed a hydrogen bond with K3.28(192) in our model. Moreover, K3.28(192) formed another two hydrogen bonds; one, an intra-molecular hydrogen bond with its own carbonyl oxygen and the other with N3.23(187) (Fig. 4B). Mutation study revealed that the binding affinity of AEA decreased an approximate 13-fold by mutating Y5.39(275) to phenylalanine, but mutating Y5.39(275) to isoleusine could abolish ligand binding and receptor signaling [23]. In addition, mutation of F3.25(189) to alanine moderately (approximately 6-fold) decreased AEA binding affinity [9]. In our model, Y5.39(275) locates very close to ACEA and should contribute to the ligand binding, as suggested by experiments. The C5=C6 double bond of ACEA interacts with F3.25(189), which was also reported previously [9].

3.1.2.1. Flexibility study of ACEA. ACEA is significantly more flexible than most drug-like compounds. A large penalty in configuration entropy is expected, which opposes binding. However, the unsaturated acyl chain of ACEA can adopt many energetically equivalent conformations that may help compensate potential entropy loss due to rigidifying the flexible compound [52]. To reveal the most rigid/flexible regions of ACEA and how the conformational changes of ACEA may affect binding, we therefore examined the changes in ACEA flexibility in three states: ACEA–CB1 bound state, free ACEA in a water box and free ACEA in vacuum. Notably, docking such a highly flexible ligand can be challenging, because the acyl chain of ACEA may cause an insufficient search for docking programs to find the best ligand-binding mode.

MD simulations were performed on ACEA in different environments: ACEA–CB1 bound state, free ACEA in a $10\,\text{Å} \times 10\,\text{Å} \times 10\,\text{Å}$ cubic TIP3P water box, and free ACEA in vacuum. Conformations were analyzed by T-Analyst. In free states, ACEA could adopt many conformations, such as extended linear structures, folded J-shape, and U-shaped conformations. In contrast, in the bound state, ACEA adopted a curved J-shape and had fewer conformations.

We computed the configurational entropy of each ACEA dihedral angle for each simulation (see Fig. 5A and B): the values for the ACEA unsaturated acyl chain were significantly lower in the bound state than the free states in water or in vacuum. Therefore, the unsaturated acyl chain of ACEA became significantly rigid after binding because of the confined binding site. Interestingly, the free ACEA in the aqueous environment was less flexible than that in vacuum, which shows diminished hydrophobic effects. The entropy of dihedrals 9 and 11 was significantly lower in the free state in water than in the bound state. Fig. 5C–E shows the distribution of dihedral 9 in the bound state and free states in water and in vacuum. In the bound state, dihedral 9 samples one more conformation than in its free form in water, where the binding site of CB1 receptor provides a more non-polar environment than in the aqueous environment. In analyzing the MD trajectories, we found that dihedral 9 acts as a "hinge" in the middle of ACEA to keep the free ACEA partially folded in water; while the long chains on both sides of the "hinge" move flexibly. In the bound state, the protein binding site confines the movement of the long acyl chain, but it brings new ACEA conformations by rearranging the "hinge", dihedral 9, to adjust the conformations of long chains on both sides. However, observed from the conformations of ACEA displayed in Fig. 5C–E, although dihedral 9 can adopt more conformations in the ACEA–CB1 bound state, the entire ligand is rigid as compared to the ACEA free states in a water box or in vacuum.

3.1.3. CB1 model trained by WIN55212-2

WIN55212-2 is a typical aminoalkylindole, with relatively more ring scaffolds and a larger structure than HU-210 and ACEA. Therefore aromatic stacking can be important for binding WIN55212-2 and its analogs to CB1 receptor [9]. Different from models built by HU-210 and ACEA, this model shows no hydrogen bonds between WIN55212-2 and K3.28(192), which agrees with mutation results [22]. In our model, WIN55212-2 is located at TMH3-5-6-7 region. An aromatic microdomain constitutes the binding region for WIN55212-2 which includes F2.61(174), F2.64(177), F3.25(189), F3.36(200), Y5.39(275), W5.43(279), W6.48(356), F7.35(379) and F3.37(381) (Tables 3 and 4 and Fig. 4C). The arrangement of residues in the binding site can be further supported by mutagenesis results, which indicated that the aromaticity of Y5.39(275) is crucial for WIN55212-2 binding [23]. McAllister and co-workers suggested that WIN55212-2 binds within TMH3-4-5-6 aromatic microdomain and directly interacts with F3.36(200), W5.43(279) and W6.48(356) with aromatic stacking [9]. In our model, residues that are in close contact with WIN55212-2 are as follows: for the naphthyl ring, F2.61(174), F2.64(177), F3.25(189), F7.35(379) and F3.37(381); for the indole ring, F3.25(189), Y5.39(275) and W5.43(279); and for the morpholinyl moiety, F3.36(200), W5.43(279) and W6.48(356). Our model showed different but more toward the "*Aroyl-up1*" WIN55212-2 binding mode compared to the binding conformations proposed by Shim and Howlett [53]. Experimental studies suggested that F3.36(200) and W5.43(279) play critical roles in providing bulky groups for WIN55212-2 binding [25]. When the aromatic residues F3.36(200), W5.43(279), and W6.48(356) were replaced by alanine, the binding of both WIN55212-2 and SR141716A to CB1 receptor was significantly reduced [54]. In addition to F3.36(200), F7.35(379) directly interacts with WIN55212-2 by aromatic stacking, and a few more aromatic stacking interactions were observed among F2.61(174), F2.64(177), F7.35(379) and F3.37(381) in our model (Tables 3 and 4).

3.1.4. CB1 model trained by SR141716A

SR141716A is the first reported CB1 antagonist that displayed nanomolar CB1 receptor affinity and stabilized the receptor in its inactive state [7]. Our SR141716A model was trained toward inactive state by 4 ns MD simulations on the ligand–CB1 complex. In this model, SR141716A locates at the TMH3-4-5-6-7 region and binds to the same aromatic microdomain with WIN55212 (Tables 3 and 5). Overall, the binding site of this model is composed of F2.61(174), F3.25(189), K3.28(192), F3.36(200), Y5.39(275), W5.43(279), W6.48(356), F7.35(379), F7.37(381), S7.39(383) and

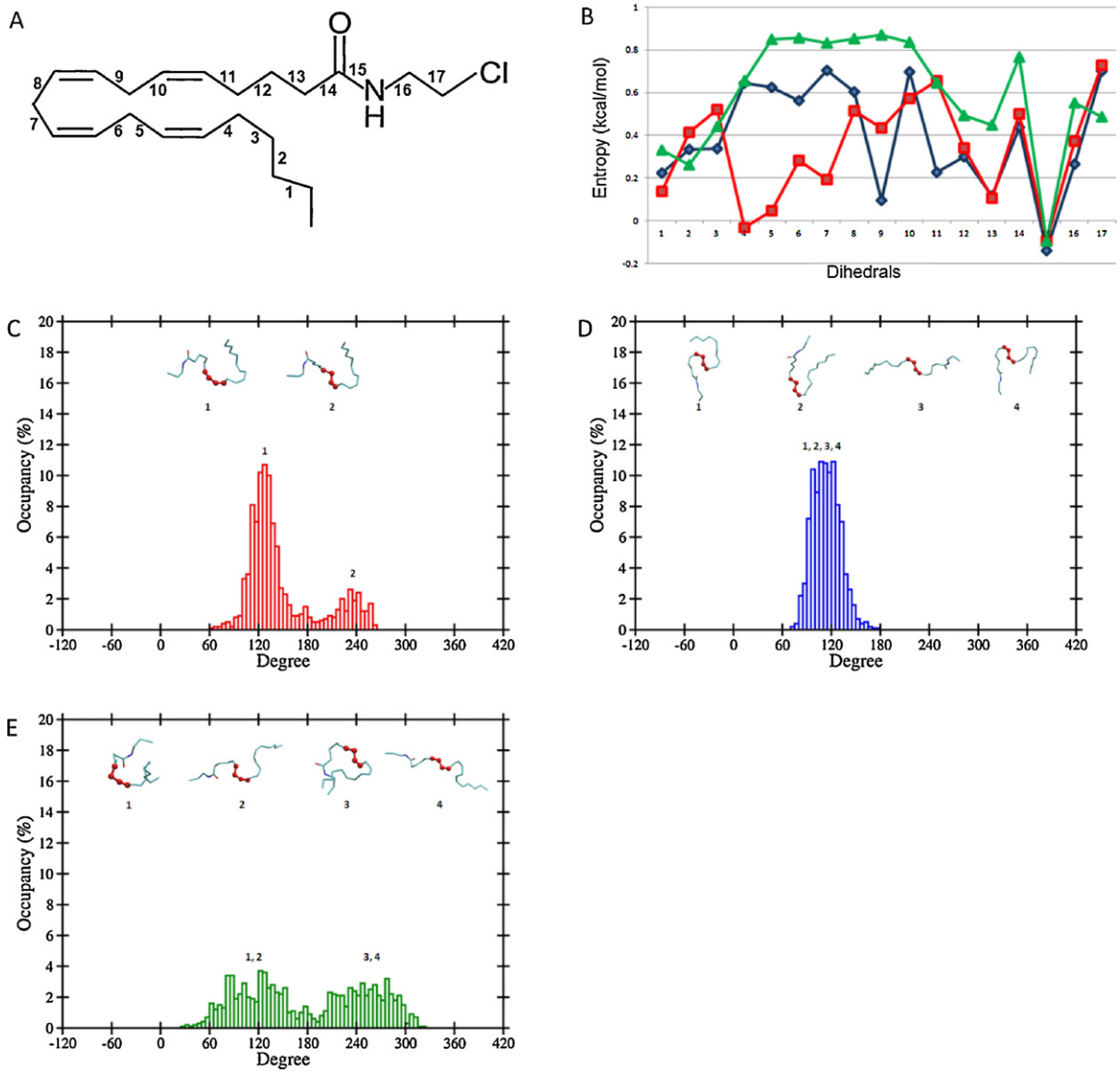

Fig. 5. Entropy and distributions of ACEA dihedrals. (A) 17 dihedrals of ACEA analyzed by T-Analyst. (B) Configurational entropy of each ACEA dihedral angle. Blue (♦) and green (▲) lines show ACEA entropy of the free ligand state in a 10 Å × 10 Å × 10 Å cubic TIP3P water box and in vacuum, respectively; red (■) line shows the entropy in the ACEA–CB1 bound state. (C–E) Distributions of dihedral 9 and ACEA conformations in (C) ACEA–CB1 bound state, (D) free state in water box and (E) free state in vacuum. (For interpretation of the references to color in this figure legend, the reader is referred to the web version of the article.)

Table 3
Key ligand-aromatic clustering in CB1 models optimized by WIN55212-2 and SR141716A.

	WIN55212-2				SR141716A			
	NAP[a]		IND[b]		MC[c]		DC[d]	
	d[e]	*α*[f]	*d*	*α*	*d*	*α*	*d*	*α*
F2.61(174)	7.99	69.57	13.45	78.96	–	–	–	–
F2.64(177)	6.15	87.40	10.90	53.29	–	–	–	–
F3.25(189)	8.19	88.53	7.98	88.23	6.22	81.98	7.91	49.68
Y5.39(275)	10.97	78.51	5.81	38.26	6.18	33.85	10.32	75.99
W5.43(279)	12.81	24.83	7.24	86.44	7.00	52.09	7.18	87.56
F7.35(379)	4.27	32.87	8.69	89.48	7.66	82.97	6.89	73.34
F3.37(381)	6.26	88.69	11.78	30.42	–	–	–	–

[a] Naphthyl ring.
[b] Indole ring.
[c] Monochlorophenyl ring.
[d] Dichlorophenyl ring.
[e] The distance between the centroids (Å).
[f] The angle between the ring planes (°).

Table 4
Key aromatic clustering in CB1 models optimized by WIN55212-2.

	F2.64(177)		F7.35(379)		F3.37(381)	
	d^a	α^b	d	α	d	α
F2.61(174)	6.86	64.06	9.25	79.72	6.16	82.31
F2.64(177)	–	–	6.54	60.75	7.78	34.70
F7.35(379)	–	–	–	–	5.03	58.22

[a] The distance between the centroids (Å).
[b] The angle between the ring planes (°).

Table 5
Key aromatic clustering in CB1 models optimized by SR141716A.

		d^a	α^b
F2.61(174)	F2.64(177)	6.75	75.19
F2.61(174)	F3.37(381)	6.40	53.83
F3.25(189)	F7.35(379)	5.13	23.82
F3.36(200)	W6.48(356)	7.42	6.42

[a] The distance between the centroids (Å).
[b] The angle between the ring planes (°).

M7.40(384) (Fig. 4D). McAllister and co-workers suggested that SR141716A binds within TMH3-4-5-6 aromatic microdomain in CB1 inactive state and directly involves aromatic stacking interactions with F3.36(200), Y5.39(275) and W5.43(279), as well as hydrogen bonding with K3.28(192) [9]. Hurst and co-workers hypothesized that, in ligand free state, the salt bridge between K3.28(192) and D6.58(366) appears to be important to position K3.28(192) for ligand interaction [55,56]. In our model, with SR141716A binding, K3.28(192) forms a hydrogen bond with the carbonyl oxygen of SR141716A and also two more hydrogen bonds with nearby N3.23(187) and S2.60(173). F3.25(189) and Y5.39(275) directly form single aromatic stacking interactions with the monochlorophenyl ring of SR141716A. W5.43(279) interacts with both the monochlorophenyl and the dichlorophenyl ring of SR141716A, which is consistent with the modeling studies by McAllister and co-workers [9]. Besides, F3.36(200), W6.48(356) and F7.35(379) interact with the dichlorophenyl ring of SR141716A. F7.35(379) directly stacks with F3.25(189) (Table 5). Mutagenesis study showed that mutation of F3.36(200), W5.43(279) or W6.48(356) to alanine significantly reduced the binding of SR141716A to the CB1 receptor [9,54,55]. Studies suggest that the interaction between F3.36(200) and W6.48(356), representing a "toggle switch", is an important constrain that keeps CB1 receptor in its inactive state and the salt bridge between K3.28(192) and D6.58(366) stabilizes CB1 in its inactive state [54,55]. In our model, F3.36(200) and W6.48(356) form a parallel-displaced stacking (Table 5) and both constitute the aromatic microdomain for SR141716A binding. Moreover, C7.42(386) is right located at the dichlorophenyl ring of SR14176A in our model while the introduction of a bulky group on C7.42(386) may inhibit SR141716A binding [57].

3.1.5. Model comparisons

Although the ligand binding sites of the four models were similar, different residues and various sidechain rearrangements characterized each binding pocket. For example, the slightly different sidechain positions of F7.35(379) and F7.37(381) could result in binding to dissimilar ligands (Fig. 6). As well, the backbones that constructed each model varied, so mobilizing sidechains in the binding site might not be enough for CB1 receptor to accept different types of ligands. The models also illustrated the flexibility of CB1 receptor and showed that multiple models were necessary for ligand screening; typical molecular docking programs cannot mobilize protein backbone structures.

3.2. CB1 receptor model validation

CB1 receptor models were assessed by docking and scoring known binders, compounds that are structurally similar to the binders and random compounds to determine whether the models could successfully rank known binders. We first performed molecular docking to place ligands into the binding site and quick energy minimization was then followed. To rank ligands, interaction energy between ligand and protein was calculated. The average binding energies for known binders, compounds with similar structure to the binders and random compounds (Table 2) validated that the four CB1 receptor homology models can distinguish known binders from the unknown compounds. Note that the energy computed does not include entropic contribution, but the binders clearly showed considerably stronger energetic attraction.

To gain insight into the ligand-induced conformational changes in the binding site of CB1 receptor, cross docking was performed by docking binders of one model to other models. Similar to model validation, energy minimization was applied, and

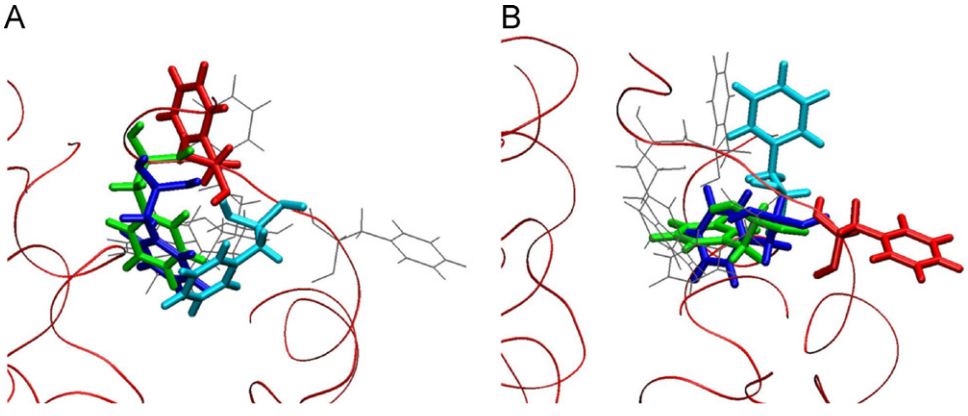

Fig. 6. Residue (A) F7.35(379) and (B) F3.37(381) in the binding sites of the four models. Red: HU-210 model; green: ACEA model; blue: WIN55212-2 model and cyan: SR141716A model. (For interpretation of the references to color in this figure legend, the reader is referred to the web version of the article.)

interaction energy was calculated to obtain average interaction energy for comparisons (see Supplementary Material, Table S2). The four CB1 receptor models could reasonably accommodate all CB1 binders, which suggests that although the models were optimized by four structurally distinguishable ligands, the binding sites maintain key characters for CB1 ligand binding. The SR141716A model has the most unique nature in failing to bind most analogs of THC and AEA but only accepts analogs of WIN55212-2, which may due to their structural similarity. Of note, SR141716A is a known CB1 antagonist. Although simulating the active and inactive CB1 receptor structures is beyond the scope of this study, the distinct SR141716A model suggests possibly substantial conformational changes between the active and inactive states of CB1 receptor.

The cross-docking results suggested that CB1 ligands may be able to bind in each optimized model. However, if a certain type of ligand was docked to a CB1 model optimized by other types of ligands, the key interactions between the ligand and CB1 receptor were rarely observed. As a result, if the scaffold of a ligand is decided, choosing a model optimized by that class of ligand is preferred. For example, if compounds with similar scaffolds as WIN55212-2 need to be screened, choosing CB1 model optimized by WIN55212-2 should be preferred. Compared with other CB1 ligands, HU-210 is relatively small in size, so the model optimized by HU-210 has the smallest binding pocket. Thus, the HU-210 model is the most ideal to screen high-affinity binders with less bulky structures. For screening compounds with linear forms, the ACEA model is the most suitable because it can accept highly flexible long acyl chains. However, ligands with flexible long chains are challenging for docking programs to find the correct binding modes, which must be carefully considered when screening ligands.

4. Conclusions

To study ligand-induced conformational changes in the CB1 receptor binding site, we constructed four homology models based on HU-210, ACEA, WIN55212-2 and SR141716A. Each of these four ligands represents one group of structurally diverse cannabinoid ligands. The interactions in the binding site of each model were carefully studied to ensure that our models reproduce known interactions suggested by experiments. Molecular docking results showed that our models can distinguish known binders from compounds with similar structures to binders and random compounds. Although all models can accept most CB1 ligands, they have preferences for different ligand scaffolds. Therefore, determining which of the four models is the most suitable one when screening a particular type of ligand can help achieve the most accurate results. The coordinates of the CB1 models are available upon request.

Acknowledgements

This work was supported in part by start-up funds from the University of California, Riverside, and the National Science Foundation (MCB-0919586).

Appendix A. Supplementary data

Supplementary data associated with this article can be found, in the online version, at http://dx.doi.org/10.1016/j.jmgm.2012.05.002.

References

[1] A.J. Kimple, D.E. Bosch, P.M. Giguere, D.P. Siderovski, Regulators of G-protein signaling and their G alpha substrates: promises and challenges in their use as drug discovery targets, Pharmacological Reviews 63 (3) (2011) 728–749.
[2] K. Mackie, Cannabinoid receptors as therapeutic targets, Annual Review of Pharmacology and Toxicology 46 (2006) 101–122.
[3] P. Pacher, S. Batkai, G. Kunos, The endocannabinoid system as an emerging target of pharmacotherapy, Pharmacological Reviews 58 (3) (2006) 389–462.
[4] R.G. Pertwee, Emerging strategies for exploiting cannabinoid receptor agonists as medicines, British Journal of Pharmacology 156 (3) (2009) 397–411.
[5] S. Ben-Shabat, L.O. Hanus, G. Katzavian, R. Gallily, New cannabidiol derivatives: synthesis, binding to cannabinoid receptor, and evaluation of their antiinflammatory activity, Journal of Medicinal Chemistry 49 (3) (2006) 1113–1117.
[6] C. Bourne, S. Roy, J.L. Wiley, B.R. Martin, B.F. Thomas, A. Mahadevan, R.K. Razdan, Novel, potent THC/anandamide (hybrid) analogs, Bioorganic & Medicinal Chemistry 15 (24) (2007) 7850–7864.
[7] P.H. Reggio, Endocannabinoid binding to the cannabinoid receptors: what is known and what remains unknown, Current Medicinal Chemistry 17 (14) (2010) 1468–1486.
[8] L.O. Hanus, R. Mechoulam, Novel natural and synthetic ligands of the endocannabinoid system, Current Medicinal Chemistry 17 (14) (2010) 1341–1359.
[9] S.D. McAllister, G. Rizvi, S. Anavi-Goffer, D.P. Hurst, J. Barnett-Norris, D.L. Lynch, P.H. Reggio, M.E. Abood, An aromatic microdomain at the cannabinoid CB1 receptor constitutes an agonist/inverse agonist binding region, Journal of Medicinal Chemistry 46 (24) (2003) 5139–5152.
[10] J.Y. Shim, W.J. Welsh, A.C. Howlett, Homology model of the CB1 cannabinoid receptor: sites critical for nonclassical cannabinoid agonist interaction, Biopolymers 71 (2) (2003) 169–189.
[11] O.M.H. Salo, M. Lahtela-Kakkonen, J. Gynther, T. Jarvinen, A. Poso, Development of a 3D model for the human cannabinoid CB1 receptor, Journal of Medicinal Chemistry 47 (12) (2004) 3048–3057.
[12] S. Durdagi, M.G. Papadopoulos, P.G. Zoumpoulakis, C. Koukoulitsa, T. Mavromoustakos, A computational study on cannabinoid receptors and potent bioactive cannabinoid ligands: homology modeling, docking, de novo drug design and molecular dynamics analysis, Molecular Diversity 14 (2) (2010) 257–276.
[13] C. Montero, N.E. Campillo, P. Goya, J.A. Paez, Homology models of the cannabinoid CB1 and CB2 receptors. A docking analysis study, European Journal of Medicinal Chemistry 40 (1) (2005) 75–83.
[14] A. Gonzalez, L.S. Duran, R. Araya-Secchi, J.A. Garate, C.D. Pessoa-Mahana, C.F. Lagos, T. Perez-Acle, Computational modeling study of functional microdomains in cannabinoid receptor type 1, Bioorganic & Medicinal Chemistry 16 (8) (2008) 4378–4389.
[15] C.-E. Chang, R. Ai, M. Gutierrez, M.J. Marsella, Homology modeling of cannabinoid receptor: discovery of cannabinoid analogues for therapeutic use, in: R. Baron (Ed.), Computational Drug Discovery and Design, vol. 819, Springer, 2012.
[16] T. Tuccinardi, P.L. Ferrarini, C. Manera, G. Ortore, G. Saccomanni, A. Martinelli, Cannabinoid CB2/CB1 selectivity. Receptor modeling and automated docking analysis, Journal of Medicinal Chemistry 49 (3) (2006) 984–994.
[17] J.Y. Shim, Transmembrane helical domain of the cannabinoid CB1 receptor, Biophysical Journal 96 (8) (2009) 3251–3262.
[18] D. Latek, M. Kolinski, U. Ghoshdastider, A. Debinski, R. Bombolewski, A. Plazinska, K. Jozwiak, S. Filipek, Modeling of ligand binding to G protein coupled receptors: cannabinoid CB(1), CB(2) and adrenergic beta(2)AR, Journal of Molecular Modeling 17 (9) (2011) 2353–2366.
[19] J.Y. Shim, Understanding functional residues of the cannabinoid CB1 receptor for drug discovery, Current Topics in Medicinal Chemistry 10 (8) (2010) 779–798.
[20] D.L. Lynch, P.H. Reggio, Cannabinoid CB1 receptor recognition of endocannabinoids via the lipid bilayer: molecular dynamics simulations of CB1 transmembrane helix 6 and anandamide in a phospholipid bilayer, Journal of Computer-Aided Molecular Design 20 (7–8) (2006) 495–509.
[21] J.-Y. Shim, A.C. Bertalovitz, D.A. Kendall, Identification of essential cannabinoid-binding domains structural insights into early dynamic events in receptor activation, Journal of Biological Chemistry 286 (38) (2011) 33422–33435.
[22] Z.H. Song, T.I. Bonner, A lysine residue of the cannabinoid receptor is critical for receptor recognition by several agonists but not WIN55212-2, Molecular Pharmacology 49 (5) (1996) 891–896.
[23] S.D. McAllister, Q. Tao, J. Barnett-Norris, K. Buehner, D.P. Hurst, F. Guarnieri, P.H. Reggio, K.W.N. Harmon, G.A. Cabral, M.E. Abood, A critical role for a tyrosine residue in the cannabinoid receptors for ligand recognition, Biochemical Pharmacology 63 (12) (2002) 2121–2136.
[24] A. Kapur, D.P. Hurst, D. Fleischer, R. Whitnell, G.A. Thakur, A. Makriyannis, P.H. Reggio, M.E. Abood, Mutation studies of Ser7.39 and Ser2.60 in the human CB1 cannabinoid receptor: evidence for a serine-induced bend in CB1 transmembrane helix 7, Molecular Pharmacology 71 (6) (2007) 1512–1524.
[25] D.F. Sitkoff, N. Lee, B.A. Ellsworth, Q. Huang, L.Y. Kang, R. Baska, Y.T. Huang, C.Q. Sun, A. Pendri, M.F. Malley, R.P. Scaringe, J.Z. Gougoutas, P.H. Reggio, W.R. Ewing, M.A. Pelleymounter, K.E. Carlson, Cannabinoid CB(1) receptor ligand binding and function examined through mutagenesis studies of F200 and S383, European Journal of Pharmacology 651 (1–3) (2011) 9–17.
[26] A.C. Howlett, F. Barth, T.I. Bonner, G. Cabral, P. Casellas, W.A. Devane, C.C. Felder, M. Herkenham, K. Mackie, B.R. Martin, R. Mechoulam, R.G. Pertwee, International union of pharmacology. XXVII. Classification of cannabinoid receptors, Pharmacological Reviews 54 (2) (2002) 161–202.
[27] R. Ai, M.Q. Fatmi, C.E.A. Chang, T-Analyst: a program for efficient analysis of protein conformational changes by torsion angles, Journal of Computer-Aided Molecular Design 24 (10) (2010) 819–827.
[28] M.P. Bokoch, Y.Z. Zou, S.G.F. Rasmussen, C.W. Liu, R. Nygaard, D.M. Rosenbaum, J.J. Fung, H.J. Choi, F.S. Thian, T.S. Kobilka, J.D. Puglisi, W.I. Weis, L. Pardo, R.S.

Prosser, L. Mueller, B.K. Kobilka, Ligand-specific regulation of the extracellular surface of a G-protein-coupled receptor, Nature 463 (7277) (2010) 108–121.
[29] V.P. Jaakola, M.T. Griffith, M.A. Hanson, V. Cherezov, E.Y.T. Chien, J.R. Lane, A.P. Ijzerman, R.C. Stevens, The 2.6 Angstrom crystal structure of a human A(2A) adenosine receptor bound to an antagonist, Science 322 (5905) (2008) 1211–1217.
[30] S.F. Altschul, T.L. Madden, A.A. Schaffer, J.H. Zhang, Z. Zhang, W. Miller, D.J. Lipman, Gapped BLAST and PSI-BLAST: a new generation of protein database search programs, Nucleic Acids Research 25 (17) (1997) 3389–3402.
[31] J. Soding, Protein homology detection by HMM-HMM comparison (vol 21, pg 951, 2005), Bioinformatics 21 (9) (2005) 2144.
[32] K. Palczewski, T. Kumasaka, T. Hori, C.A. Behnke, H. Motoshima, B.A. Fox, I. Le Trong, D.C. Teller, T. Okada, R.E. Stenkamp, M. Yamamoto, M. Miyano, Crystal structure of rhodopsin: a G protein-coupled receptor, Science 289 (5480) (2000) 739–745.
[33] T. Okada, M. Sugihara, A.N. Bondar, M. Elstner, P. Entel, V. Buss, The retinal conformation and its environment in rhodopsin in light of a new 2.2 angstrom crystal structure, Journal of Molecular Biology 342 (2) (2004) 571–583.
[34] S.G.F. Rasmussen, H.-J. Choi, D.M. Rosenbaum, T.S. Kobilka, F.S. Thian, P.C. Edwards, M. Burghammer, V.R.P. Ratnala, R. Sanishvili, R.F. Fischetti, G.F.X. Schertler, W.I. Weis, B.K. Kobilka, Crystal structure of the human beta(2) adrenergic G-protein-coupled receptor, Nature 450 (7168) (2007) 383–384.
[35] V. Cherezov, D.M. Rosenbaum, M.A. Hanson, S.G.F. Rasmussen, F.S. Thian, T.S. Kobilka, H.J. Choi, P. Kuhn, W.I. Weis, B.K. Kobilka, R.C. Stevens, High-resolution crystal structure of an engineered human beta(2)-adrenergic G protein-coupled receptor, Science 318 (5854) (2007) 1258–1265.
[36] C. Notredame, D.G. Higgins, J. Heringa, T-Coffee: a novel method for fast and accurate multiple sequence alignment, Journal of Molecular Biology 302 (1) (2000) 205–217.
[37] D.T. Jones, Protein secondary structure prediction based on position-specific scoring matrices, Journal of Molecular Biology 292 (2) (1999) 195–202.
[38] K. Arnold, L. Bordoli, J. Kopp, T. Schwede, The SWISS-MODEL workspace: a web-based environment for protein structure homology modelling, Bioinformatics 22 (2) (2006) 195–201.
[39] A.E. Torda, J.B. Procter, T. Huber, Wurst: a protein threading server with a structural scoring function, sequence profiles and optimized substitution matrices, Nucleic Acids Research 32 (2004) W532–W535.
[40] G.G. Krivov, M.V. Shapovalov, R.L. Dunbrack, Improved prediction of protein side-chain conformations with SCWRL4, Proteins-Structure, Function, and Bioinformatics 77 (4) (2009) 778–795.
[41] W. Humphrey, A. Dalke, K. Schulten, VMD: visual molecular dynamics, Journal of Molecular Graphics 14 (1) (1996) 33–38.
[42] J.C. Phillips, R. Braun, W. Wang, J. Gumbart, E. Tajkhorshid, E. Villa, C. Chipot, R.D. Skeel, L. Kale, K. Schulten, Scalable molecular dynamics with NAMD, Journal of Computational Chemistry 26 (16) (2005) 1781–1802.
[43] J.W. Ponder, D.A. Case, Force fields for protein simulations, Advances in Protein Chemistry 66 (2003) 27–85.
[44] A.C. Bertalovitz, K.H. Ahn, D.A. Kendall, Ligand binding sensitivity of the extracellular loop two of the cannabinoid receptor 1, Drug Development Research 71 (7) (2010) 404–411.
[45] J.-Y. Shim, J. Rudd, T.T. Ding, Distinct second extracellular loop structures of the brain cannabinoid CB(1) receptor: implication in ligand binding and receptor function, Proteins-Structure, Function, and Bioinformatics 79 (2) (2011) 581–597.
[46] V. Kairys, M.K. Gilson, Enhanced docking with the mining minima optimizer: acceleration and side-chain flexibility, Journal of Computational Chemistry 23 (16) (2002) 1656–1670.
[47] D.A. Case, T.A. Darden, T.E. Cheatham, C.L. Simmerling, J. Wang, R.E. Duke, R. Luo, R.C. Walker, W. Zhang, K.M. Merz, B.P. Roberts, B. Wang, S. Hayik, A. Roitberg, G. Seabra, I. Kolossvai, K.F. Wong, F. Paesani, J. Vanicek, J. Liu, X. Wu, S.R. Brozell, T. Steinbrecher, H. Gohlke, Q. Cai, X. Ye, J. Wang, M.J. Hsieh, G. Cui, D.R. Roe, D.H. Mathews, M.G. Seetin, C. Sagui, V. Babin, T. Luchko, S. Gusarov, A. Kovalenko, P.A. Kollman, AMBER 11, University of California, San Francisco, 2010.
[48] G.M. Morris, D.S. Goodsell, R.S. Halliday, R. Huey, W.E. Hart, R.K. Belew, A.J. Olson, Automated docking using a Lamarckian genetic algorithm and an empirical binding free energy function, Journal of Computational Chemistry 19 (14) (1998) 1639–1662.
[49] O. Trott, A.J. Olson, Software news and update AutoDock Vina: improving the speed and accuracy of docking with a new scoring function, efficient optimization, and multithreading, Journal of Computational Chemistry 31 (2) (2010) 455–461.
[50] J.J. Irwin, B.K. Shoichet, ZINC – a free database of commercially available compounds for virtual screening, Journal of Chemical Information and Modeling 45 (1) (2005) 177–182.
[51] R.P. Picone, A.D. Khanolkar, W. Xu, L.A. Ayotte, G.A. Thakur, D.P. Hurst, M.E. Abood, P.H. Reggio, D.J. Fournier, A. Makriyannis, (−)-7′-isothiocyanato-11-hydroxy-1′,1′-dimethylheptylhexahydrocannabinol (AM841), a high-affinity electrophilic ligand, interacts covalently with a cysteine in helix six and activates the CB1 cannabinoid receptor, Molecular Pharmacology 68 (6) (2005) 1623–1635.
[52] M. van der Stelt, J.A. van Kuik, M. Bari, G. van Zadelhoff, B.R. Leeflang, G.A. Veldink, A. Finazzi-Agro, J.F.G. Vliegenthart, M. Maccarrone, Oxygenated metabolites of anandamide and 2-arachidonoylglycerol: conformational analysis and interaction with cannabinoid receptors, membrane transporter, and fatty acid amide hydrolase, Journal of Medicinal Chemistry 45 (17) (2002) 3709–3720.
[53] J.Y. Shim, A.C. Howlett, WIN55212-2 docking to the CB1 cannabinoid receptor and multiple pathways for conformational induction, Journal of Chemical Information and Modeling 46 (3) (2006) 1286–1300.
[54] S.D. McAllister, D.P. Hurst, J. Barnett-Norris, D. Lynch, P.H. Reggio, M.E. Abood, Structural mimicry in class A G protein-coupled receptor rotamer toggle switches – the importance of the F3.36(201)/W6.48(357) interaction in cannabinoid CB1 receptor activation, Journal of Biological Chemistry 279 (46) (2004) 48024–48037.
[55] P.H. Reggio, Toward the design of cannabinoid CB1 receptor inverse agonists and neutral antagonists, Drug Development Research 70 (8) (2009) 585–600.
[56] D.P. Hurst, D.L. Lynch, J. Barnett-Norris, S.M. Hyatt, H.H. Seltzman, M. Zhong, Z.H. Song, J.J. Nie, D. Lewis, P.H. Reggio, N-(Piperidin-1-yl)-5-(4-chlorophenyl)-1-(2,4-dichlorophenyl)-4-methyl-1H-pyrazole-3-carboxamide (SR 141716A) interaction with LYS 3.28(192) is crucial for its inverse agonism at the cannabinoid CB1 receptor, Molecular Pharmacology 62 (6) (2002) 1274–1287.
[57] J.F. Fay, T.D. Dunham, D.L. Farrens, Cysteine residues in the human cannabinoid receptor: only C257 and C264 are required for a functional receptor, and steric bulk at C386 impairs antagonist SR 141716A binding, Biochemistry 44 (24) (2005) 8757–8769.